Considerations Regarding Bearingless Flux-Switching Slice Motors

W. Gruber[1], W. Bauer[1], K. Radman[2] W. Amrhein[1]and R. T. Schöb[3]
[1] Johannes Kepler University Linz, Austria
wolfgang.gruber@jku.at, walter.bauer@jku.at, wolfgang.amrhein@jku.at
[2] University Rijeka, Croatia
karlor@riteh.hr
[3] Levitronix GmbH, Zurich, Switzerland
rschoeb@levitronix.com

Abstract

The bearingless flux-switching slice motor is a compact magnetically levitated drive featuring no permanent magnets in the rotor. In this article the working principle of this novel bearingless motor topology is studied and its operational behavior is evaluated using performance factors for bearing and torque generation. Three dimensional finite element simulations are performed to optimize a promising motor variant, showing encouraging results, that will be verified in the future with the help of a prototype.

1 Introduction

The term bearingless motor describes the combined generation of motor torque and bearing forces by only one single device. Often in magnetically levitated drives the mechanical bearings are replaced by magnetic ones and, thus, the integration of the driving functionality is not considered. Bearingless motors have been developed in the early 1990ies. The leading role had the ETH Zurich in Switzerland [1] and the University of Tokyo in Japan [2].

The advantages of magnetic suspension lie in the contact-free operation of stator and rotor. Hence, no abrasion and no wear take place, leading to no inherent contamination. Additionally, hermetically sealed systems without lubrication and sealing can be realized. The rotation speed is not limited by the bearing itself. Compared to magnetically levitated drives, bearingless motors feature a very compact mechanical setup and allow the active control of multiple degrees of freedom at relatively low price. This is the reason for an increased research in this field, which has led to several industrial products [3].

2 Bearingless Slice Motor

Using an air gap field featuring permanent magnetic bias flux and a disc-shaped rotor, it becomes possible to stabilize three degrees of freedom (the two tilting and the axial displacement) passively by reluctance forces. This principle is illustrated in Fig. 1. The active control of the remaining three degrees of freedom (the radial movements and the rotation) by the stator coils results in a fully magnetically levitated drive. Such systems are called bearingless slice motors and were first introduced in 1995 [4]. Steady development led to industrial applications of these drives, mainly as pumps in the medical and semiconductor industry [5], [6].

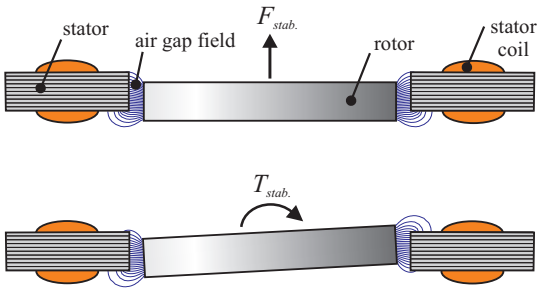

Figure 1. Principle of passive stabilization due to permanent magnetic reluctance forces: axial movement (top) and tilting deflection (bottom)

However, in state-of-the art bearingless slice motors the permanent magnets exciting the air gap bias flux are located in the rotor [7]. Thus, the rotor cross section of bearingless motors shows a strong affinity to rotors of brushless permanent magnet synchronous machines. The stator winding systems are often separated. This means, that there is one winding system creating only bearing forces and another one generating only driving torque. Both are wound on the stator. Alternatively, the use of one common winding system, creating both combined bearing forces and motor torque is feasible. For a proper operation it is necessary to decouple bearing forces and motor torque accordingly. This is achieved by a sophisticated nonlinear control scheme. However, the use of only one winding system normally simplifies the mechanical manufacture and additionally reduces the copper losses by approximately 30% [8].

Especially in high temperature or high speed applications and in disposable devices (where the rotor has to be replaced frequently) permanent magnet free rotors would be favourable. Using a magnetless rotor setup leads to reduced manufacturing costs (the state-of-the-art rare earth magnet materials have increased their price significantly in the last years) and increased thermal and mechanical robustness. First studies concerning bearingless slice motors without magnetic material in the rotor, also called bearingless reluctance slice motor, were published recently in [9] and [10]. The motor variant considered in this work, the bearingless flux-switching slice drive, poses an additional promising possibility to realize such a system.

3 Flux-Switching Drive

The main constructional characteristic of the flux-switching motor, depicted in Fig. 2, is the placement of the permanent magnets. They are located in the midst of the stator teeth and separate them electromagnetically. The flux lines of each permanent magnets close mainly over the neighbouring stator teeth and, thus, do not penetrate the whole air gap, but only influence the air gap region close to the permanent magnet. Unfortunately, there is also a considerable amount of fringing flux closing over the outer side of the stator. To keep this kind of stray flux low, a small air gap length (compared to the magnet width) is favourable and necessary.

However, the air gap flux density in flux-switching machines is often higher than in comparable other electric machines, leading to an increased torque capability [12]. This is due to the flux concentration capability of the construction. As indicated in Fig. 3, the surfaces of the stator teeth normal to the magnetization direction collect permanent magnetic flux and concentrate it towards the much smaller area of the stator teeth adjoining the air gap. Due to the saliency of the rotor, the flux linked with the stator coils changes its direction, resulting in an induced stator back electromagnetic force voltage, a necessity for permanent magnetic torque generation. This behaviour is visible in

Fig 3. Additionally, the superposition of the stator field with the permanent magnetic field also leads to a creation of bearing forces. In the next section a mathematical description for this kind of torque and force generation will be given.

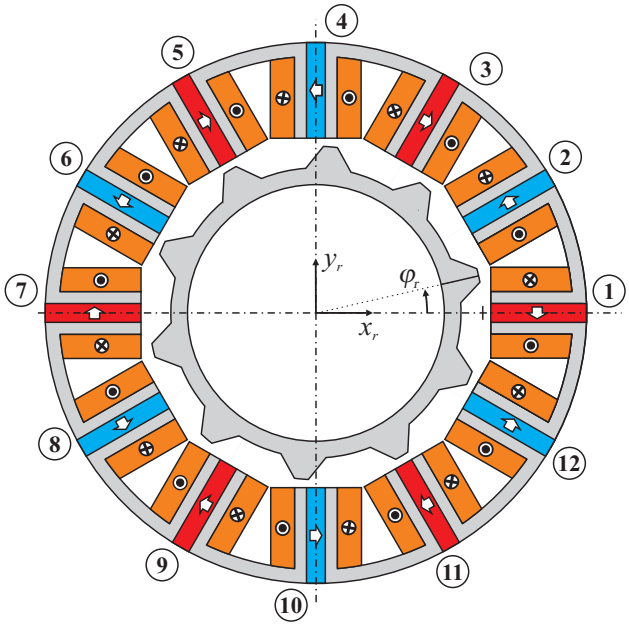

Figure 2. Cross section of a flux-switching motor with twelve stator and ten rotor teeth. The arrows indicate the direction of the magnetization.

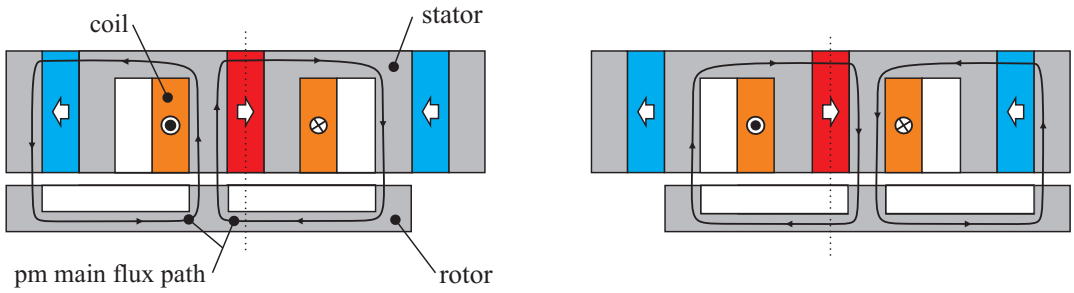

Figure 3 Principle of motor torque generation in flux switching drives: The salient pole rotor creates an alternating permanent magnetic flux in the stator coils during rotation.

4 Mathematical Model

4.1 Bearing Force and Motor Torque Generation

The suspension forces F_x and F_y and the drive torque T_z that are created from the phase currents can be described by

$$\begin{pmatrix} F_x(\varphi_r) \\ F_y(\varphi_r) \\ T_z(\varphi_r) \end{pmatrix} = \begin{pmatrix} \mathbf{i}_s^{\mathrm{T}} & \mathbf{0} & \mathbf{0} \\ \mathbf{0} & \mathbf{i}_s^{\mathrm{T}} & \mathbf{0} \\ \mathbf{0} & \mathbf{0} & \mathbf{i}_s^{\mathrm{T}} \end{pmatrix} \mathbf{T}_Q(\varphi_r)\mathbf{i}_s + \mathbf{T}_L(\varphi_r)\mathbf{i}_s + \mathbf{T}_C(\varphi_r). \tag{1}$$

This description [13] demands linear material behaviour and therefore neglects saturation effects. Additionally centred rotor position is presumed. All phase currents are combined into the stator current vector $\mathbf{i}_s$ and φ_r represents the angular position of the rotor. However, in (1) three parts are visible, which add up to create the bearing forces and the motor torque. The vector $\mathbf{T}_C(\varphi_r)$ is the only part that is independent from the stator currents and describes the reluctance forces due to the permanent magnet and the cogging torque. The term with linear dependency from the stator current with $\mathbf{T}_L(\varphi_r)$ represents the forces and torque that are created due to the mutual interaction of permanent magnetic field and stator current field. In permanent magnetic machines this part is normally dominant. Finally, the last contingent with $\mathbf{T}_Q(\varphi_r)$ is influenced by the stator current alone and is therefore also present without any permanent magnets. This part is used in standard magnetic bearings or common reluctance machines. However, it features a nonlinear, quadratic dependency from the stator currents.

4.2 Decoupling of Force and Torque

For a proper bearingless motor operation the phase currents have to be computed in order to create certain bearing forces in x_r- and y_r-direction as well as to generate motor torque. Thus, these values have to be decoupled properly in dependence of the rotor angle. A possible solution for this problem is given by the pseudo-inverse

$$\mathbf{K}_L(\varphi_r) = \mathbf{T}_L(\varphi_r)^T \left(\mathbf{T}_L(\varphi_r)\mathbf{T}_L(\varphi_r)^T \right)^{-1}, \tag{2}$$

deduced detailed in [14]. The computed phase current vector $\mathbf{i}_s=\mathbf{K}_L(\varphi_r)\cdot(F_x\ F_y\ M_z)^T$ results in the desired suspension force (F_x and F_y) and torque (M_z) generation with the lowest possible resistive copper losses.

It is important to stress that this computation postulates a dominant term with linear current dependency in (1), because the principle of superposition is applied. Therefore, the reluctance forces have to be small. In drives and rotors with significant saliency this necessity is not fulfilled automatically and also cannot be guaranteed for the flux-switching motor. Taking a closer look at permanent magnet excited drives it becomes clear that the disturbing reluctance forces are dependent on the rotor angle. Additionally, in most cases the reluctance forces are strong only in radial direction towards the energized coil. In tangential direction and in the drive torque the quadratic reluctance terms are negligible in most cases.

However, the disturbing reluctance components can be annihilated by proper connection of two opposing coils into one phase. Figure 4 illustrates the basic principle. When two opposing coils are connected concordant in series as depicted in Fig 4a), two force vectors are created, that are equal but shifted exactly by 180° due to symmetry. An even number of rotor teeth has to be postulated additionally. Hence, when all forces are superposed, no resulting forces remain but motor torque is created. In a similar way Fig. 4b) shows two opposing and inversely connected coils in series. This

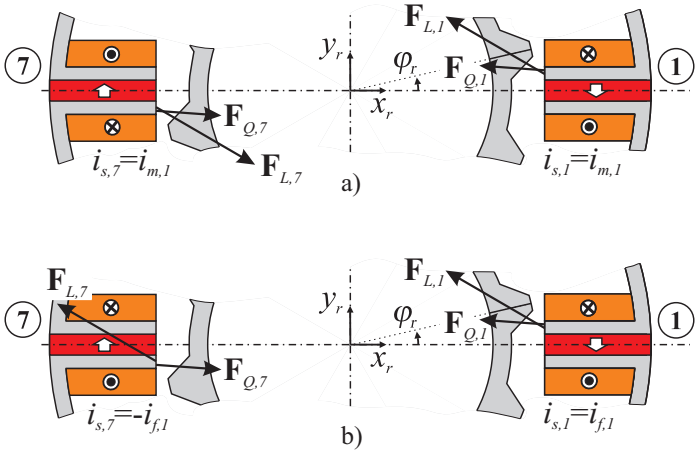

Figure 4. Decoupling of bearing force and drive torque generation and elimination of nonlinear reluctance components by the proper phase connection of opposing coils: a) concordant flux linkage leads to pure torque generation; b) inversely arranged flux linkage results in linear supsension force creation

setup leads to a duplication of the linear force parts $\mathbf{F}_L$ and an annihilation of the quadratic force components $\mathbf{F}_Q$. No torque is created in this case.

The described approach relies on an even number of stator and rotor teeth to connect opposing coil pairs properly into separated bearing and torque phases. Acting on the assumption of a double 2-phase winding system with non overlapping coils for bearing and torque generation, at least 8 stator teeth are necessary. For a double 3-phase winding system at least 12 stator teeth are required.

5 Evaluation of Bearingless Flux-Switching Motor Topologies

5.1 Performance Factors

Favorable combinations regarding the number of stator and rotor teeth for regular flux-switching motors (with mechanical bearings) have been studied and discussed in [15]. In this section a similar investigation is conducted for bearingless flux-switching machines. Thus, both motor and bearing behavior have to be considered. For this reason, performance factors are defined that will help to evaluate the operational characteristic of each considered motor topology.

As mentioned before, the matrix $\mathbf{K}_L(\varphi_r)$ allows the computation of the phase currents needed to generate a specific suspension force and certain motor torque by

$$\mathbf{i}_s(\varphi_r) = \mathbf{K}_L(\varphi_r)\begin{pmatrix} F_x \\ F_y \\ T_z \end{pmatrix} \tag{3}$$

in dependence of the rotor angle. When the currents to create force and torque are relatively small, the bearingless motor features generally a better functionality than systems that need higher coil currents. Thus, the entries of the $\mathbf{K}_L(\varphi_r)$ allow a prediction of the motors ability to generate bearing forces and motor torque. The first column for instance describes the necessary currents for the creation of suspension forces in x_r-direction and the second column for force generation in y_r-direction. Hence, as performance factor for suspension force generation the inverse value of the maximum entry of the first

two columns can be used. Due to the fact that higher phase systems are featuring a higher amount of opposing coils, they will also create higher forces and torque. Hence a normalization (referencing the performance factor to the number of used opposing coils pairs) makes sense. Therefore, the following force performance factor

$$k_f = \frac{F_{overall,min}}{F_{phase,max}} \frac{4}{N_{s,f}} = \min_{i=1,2} \left(\frac{1}{\max_{j,\varphi_r} \left| k_{L,ij}(\varphi_r) \right|} \right) \frac{4}{N_{s,f}} \tag{4}$$

is defined, where $k_{L,ij}(\varphi_r)$ describes the entry in the i-th column and j-th row in the $\mathbf{K}_L(\varphi_r)$-matrix. $N_{s,f}$ stands for the number of stator teeth that hold coils used for force creation. In an analogue way it is possible to define the torque performance factor

$$k_t = \frac{T_{overall,min}}{T_{phase,max}} \frac{4}{N_{s,t}} = \frac{1}{\max_{j,\varphi_r} \left| k_{L,3j}(\varphi_r) \right|} \frac{4}{N_{s,t}} . \tag{5}$$

In this equation $N_{s,t}$ represents the number of stator teeth holding coils, that are used to generator motor torque. Both performance factors can be considered to be normalized, when the entries of the $\mathbf{T}_L(\varphi_r)$-matrix, used to compute $\mathbf{K}_L(\varphi_r)$, are also normalized. Small performance factors (4) and (5) indicate a poor force and torque capability of the considered bearingless motor (at least at a certain rotor angles). However, often torque ripples or single phase torque characteristic (and therefore small or even zero values of k_t) are acceptable. In contrast to that, small force performance factors k_f are inadmissible for proper bearingless motor operation.

5.2 One Phase Operational Behavior

It was mentioned in chapter 3, that a turning rotor induces an alternating permanent magnetic flux in a stator coils due to its saliency. This alternating flux is duplicated in phases, which are connected according to Fig. 4a). In contrast to that the induced permanent magnetic flux cancels out in coil connections depicted in Fig. 4b) used for force generation.

It is well known that the phase torque part with linear dependency on the coil current results from the angular derivative of the linked stator phase flux $\Psi_{PM,phase}$, yielding

$$T_{L,phase}(\varphi_r) = \frac{\partial \Psi_{PM,phase}}{\partial \varphi_r} i_{s,phase} . \tag{6}$$

Hence, for constant current linkage in the torque phase an approximately sinusoidal torque characteristic over the rotor angle is obtained, as illustrated in Fig. 5.

The suspension force created by one force phase of the flux-switching motor is separated into two components in normal and tangential direction with reference to the axis of the considered opposing coil pair. In contrast to standard active magnetic bearings an alternating normal force component is observed due to the permanent magnetic bias flux that is strengthened or weakened in dependence of the rotor angle. The force generation is doubled due to the proper connection of the opposing coils and its characteristic is assumed to be sinusoidal. Figure 6 illustrates the described behaviour.

The monitored tangential forces also vary due to the saliency of the rotor in a sinusoidal way over the rotor angle. Additionally, the tangential force component (directed towards y_r-direction in Fig. 4b)) features a considerable constant force component. This results from the fact that for current creation both opposing coil pairs feature field weakening on the same side of the x_r-axis, either above or below, leading to unsymmetrical biased air gap field and a tangential draft on the rotor.

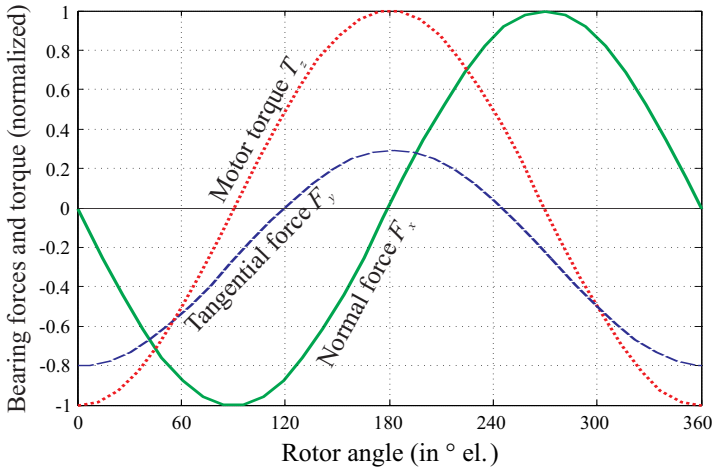

Figure 5. Bearing force and motor torque (acting on the rotor) with proper connection of opposing coils with constant flux linkage over the rotor angle (only the fundamental wave is considered and the curves are normalized)

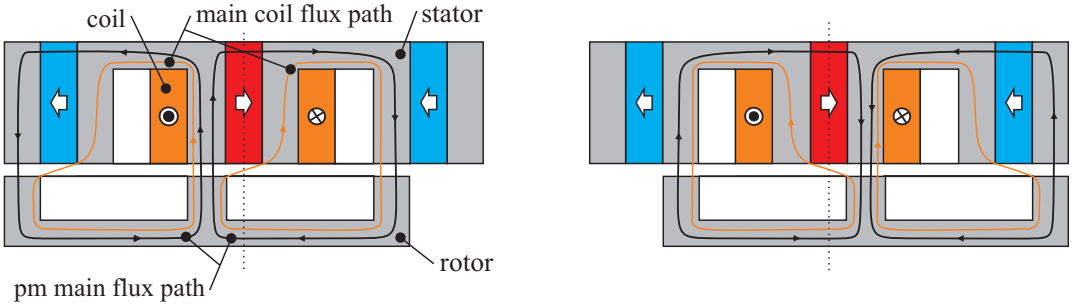

Figure 6. Basic principle of bearing force generation in flux-switching drives: The coils flux superimposes the permanent magnetic flux at different rotor positions: field strengthening (left); field-weakening (right)

The characteristic curves from Fig. 5 hold true for the sense of winding and the permanent magnet magnetization direction inside the stator teeth that are visible in Fig. 4. When either the magnetization direction or the winding direction is changed, the signs of all three characteristic curves in Fig. 5 have to be switched.

5.3 Overall Drive Characteristic

For the considered kind of bearingless drives at least two phases for torque and two phases for suspension force are necessary for proper operation. The connection of opposing coils, as depicted in Fig. 4, requires at least two opposing stator teeth per phase. Hence, at least 8 stator teeth are necessary for a double 2-phase system. Using a double 3-phase winding system requires a minimum of 12 stator teeth. These two stator topologies are examined in the following. Mixed systems, e. g. a 2-phase suspension force winding system combined with a 3-phase torque winding system, which would have at least 10 stator teeth, are not considered in this paper.

Concerning the rotor it was explained before that only an even number of rotor teeth N_r are useable. Additionally, the number of rotor teeth is not allowed to differ too much from the number of stator teeth N_s due to geometric reasons. This fact is well known from state-of-the-art reluctance drives.

Winding Topologies

The studied winding topologies of the following section are illustrated in Fig. 7. They are characterized by their full symmetric arrangement. When winding arrangements, that are only symmetric around one axis are accepted, a lot more winding variants are feasible, but these are normally of minor importance. The double 2- and 3-phase systems visible in Fig. 7a) and 7b) are obvious winding topologies. The winding schemes depicted in Fig. 7c) and 7d) are explained in detail.

In Fig. 7c) a double 2-phase winding system is indicated. The single phases differ in the number of coils per phase. There are two coils each in the phases U_1 und V_1 and four coils each in the phases U_2 und V_2. It is important to note, that there is a difference in the overall system performance whether the first winding systems (U_1V_1) or the second winding system (U_2V_2) is used to generator torque or suspension forces, respectively. Depending on this choice, the resulting connection of the opposing coil pairs (indicated with the indices a and b in Fig. 7c) and 7d)) will result immediately. Above that there are two ways to combine the two coil pairs of the second winding system (U_2V_2, consisting of for four single coils each). The two pairs can be connected in the same or in the opposing direction. Thus, all in all the winding systems illustrated in Fig. 7c) and 7d) represent four different possible bearingless slice motor variants each.

Performace Factors

Using the normalized phase characteristic of the bearing force and drive torque phases, obtained from properly connected opposing coil pairs, the performance factors can be computed for each of the considered bearingless flux-switching slice motor topologies in dependence of the number of rotor teeth. These factors reflect the operational behaviour of the different bearingless flux-switching motor variants. Thus, a comparison and analysis of the different topologies becomes feasible. The

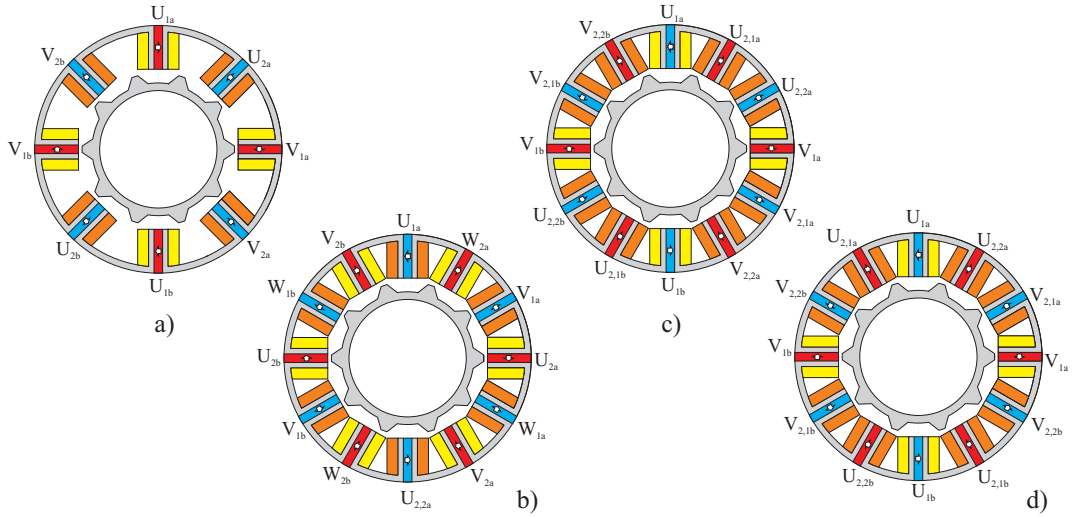

Figure 7. Considered winding systems for decoupled force and torque generation: a) features a double 2-phase-system (U_1V_1 and U_2V_2) for N_s=8; b) shows a double 2-phase-system $U_1V_1W_1$ und $U_2V_2W_2$) for N_s=12; c) and d) depict additional 2-phase

computation of the overall $\mathbf{T}_L(\varphi_r)$-matrix from the normalised phase-characteristic, displayed in Fig. 5, is explained and deduced in [9]. Once $\mathbf{T}_L(\varphi_r)$ is known, it is easy to compute $\mathbf{K}_L(\varphi_r)$ by (2). The finally obtained force and torque performance factors for each drive topology are summarized in Table I. It is remarkable, that in all 2-phase systems the torque performance factor k_m is zero. This means that there is at least one rotor angle, in which no torque creation is possible. This behaviour is also called single phase drive characteristic. This motor characteristic might be problematic because it features high torque ripple and measures must be taken to guarantee a reliable run-up of the drive. However, in a lot of industrial applications, e. g. for fans, blowers or pumps, single phase characteristic is of minor importance and certainly acceptable. In contrast to drives with single phase characteristic, that are capable to create mean torque over the rotor angle and that are indicated in Table I with k_t=0.0, there are also two considered drive topologies with N_r=12 that cannot create any torque at all. In order to point out the difference, these systems were benchmarked with k_m=0.

In contrast to the torque performance factor it is not acceptable for the force performance factor to be small in bearingless motors. Small force factors indicate that the drive is not capable to generate bearing forces properly at least at a certain rotor angle. Experience teaches that such drives cannot be used as bearingless motors appropriately and therefore cannot be used. Thus, topologies with small force factors have been marked with red background in Table I to indicate their inapplicability. On the other hand flux-switching drive variants that feature high performance factors have been marked in green.

Evaluating the performance factors, it was decided to take a closer look at the double 3-phases flux-switching drive variant with 12 stator teeth and 10 rotor teeth. It is known that this topology is capable to create high torque (k_t=1.0), and due to the relatively high force factor of k_f=0.57 also a bearingless operation looks promising. In the next chapter the prototype design and optimization of this drive topology is outlined.

TABLE I OPERATIONAL BEHAVIOUR OF THE FLUX-SWITCHING BEARINGLESS SLICE MOTOR

winding (Fig. 7)	***Stator teeth (N_s=8)***				
	N_r=4	***N_r=6***	***N_r=8***	***N_r=10***	***N_r=12***
a)	k_f=0.33 k_t=0.0	k_f=0.33 k_t=0.0	k_f=0.33 k_t=0.0	k_f=0.33 k_t=0.0	k_f=0.33 k_t=0.0
	Stator teeth (N_s=12)				
	N_r=8	***N_r =10***	***N_r =12***	***N_r=14***	***N_r=16***
b)	k_f=0.0 k_t=1.0	k_f=0.57 k_t=1.0	k_f=0.33 k_t=0.0	k_f=0.0 k_t=1.0	k_f=0.57 k_t=1.0
c) U_1=U_t $\theta_{2,1a}$= $\theta_{2,2a}$	k_f=0.35 k_t=0.0	k_f=0.0 k_t=0.0	k_f=0.1 k_t=0.0	k_f=0.5 k_t=0.0	k_f=0.6 k_t=0.0
c) U_1=U_t $\theta_{2,1a}$= $\theta_{2,2b}$	k_f=0.27 k_t=0.0	k_f=0.38 k_t=0.0	k_f=0.32 k_t=0.0	k_f=0.12 k_t=0.0	k_f=0.18 k_t=0.0
c) U_1=U_f $\theta_{2,1a}$= $\theta_{2,2a}$	k_f=0.33 k_t=0.0	k_f=0.33 k_t=0.0	k_f=0.33 k_t=0	k_f=0.33 k_t=0.0	k_f=0.33 k_t=0.0
c) U_1=U_f $\theta_{2,1a}$=$\theta_{2,2b}$	k_f=0.33 k_t=0.0	k_f=0.33 k_t=0.0	k_f=0.33 k_t=0.0	k_f=0.33 k_t=0.0	k_f=0.33 k_t=0.0
d) U_1=U_t $\theta_{2,1a}$=$\theta_{2,2a}$	k_f=0.0 k_t=0.0	k_f=0.48 k_t=0.0	k_f=0.3 k_t=0.0	k_f=0.0 k_t=0.0	k_f=0.48 k_t=0.0
d) U_1=U_t $\theta_{2,1a}$=$\theta_{2,2b}$	k_f=0.67 k_t=0.0	k_f=0.08 k_t=0.0	k_f=0.17 k_t=0.0	k_f=0.63 k_t=0.0	k_f=0.18 k_t=0.0
d) U_1=U_f $\theta_{2,1a}$=$\theta_{2,2a}$	k_f=0.33 k_t=0.0	k_f=0.33 k_t=0.0	k_f=0.33 k_t=0.0	k_f=0.33 k_t=0.0	k_f=0.33 k_t=0.0
d) U_1=U_f $\theta_{2,1a}$=$\theta_{2,2b}$	k_f=0.33 k_t=0.0	k_f=0.33 k_t=0.0	k_f=0.33 k_t=0	k_f=0.33 k_t=0.0	k_f=0.33 k_t=0.0

6 Prototype Design

Before the optimization with finite element simulation runs war started, certain geometric parameters were set. The air gap δ was fixed with 3mm and the rotor outer diameter d_{ra} determined to be 150mm. All the other tuneable parameters are depicted in Fig. 8.

6.1 Finite Elemente Simulations

A 3D finite element optimization of the geometry was conducted with the software package Maxwell 3D from Ansoft. Previous works [16], [17] optimized the geometric parameters of standard (non bearingless) flux-switching motors with respect to torque generation. From these papers favourable geometric parameters are known, for instance a recommendation to set the rotor to stator diameter ratio between 0.55 and 0.6 is given. Additionally, it is favourable to have an approximately equal stator tooth width, magnet width and stator slot width, whereas the rotor tooth width should be about 1.4 times bigger than the stator tooth width.

However, beside the maximization of the motor torque also the increase of the passive stabilizing stiffnesses and the bearing forces are optimization criteria. During the finite element simulations it turned out that saturation effects restrict the parameter choice, especially of the stator geometry. Due to the limited design space, saturation effects occur in the iron of the stator teeth (at higher current densities or torque creation, respectively). Hence, the geometry was adopted accordingly. The iron of the stator tooth was increased and the outer stator diameter decreased to reduce the magnetic flux density. Figure 9 shows, that with these measures a flux density of 1.5T is reached at maximum flux linkage in the coils, what is still close to saturation. Table II summarizes the geometric values of the prototype that have been obtained from the finite element optimization runs.

The simulated force and torque characteristics of one bearing and one torque phase at constant flux linkage represent on column of the $\mathbf{T}_L(\varphi_r)$-matrix. Due to symmetry, from this data the overall the $\mathbf{T}_L(\varphi_r)$-matrix can be computed, as described in [9]. Using (2), $\mathbf{K}_L(\varphi_r)$ can be deduced, allowing to compute all necessary phase coils for a certain torque and/or bearing force generation. The finite element simulation model has been energized with these computed phase currents for certain points of

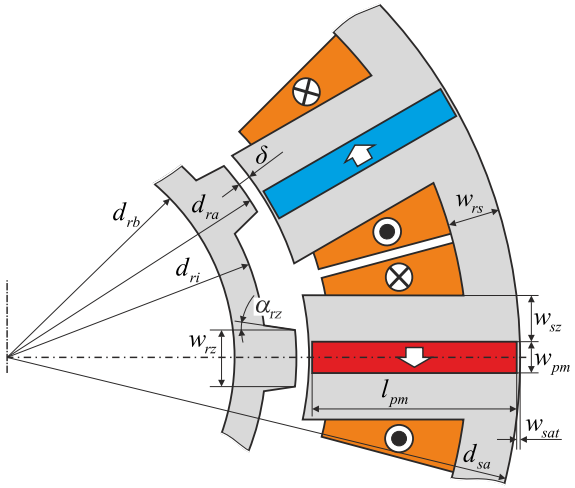

Figure 8. Designation of the geometry parameters of the flux-switching bearingless slice motor with 12 stator and 10 rotor teeth

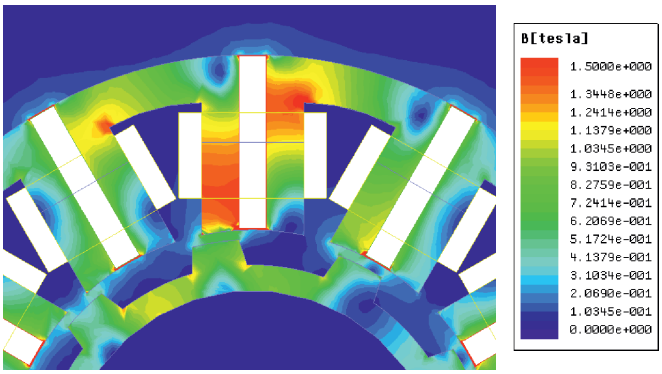

Figure 9. Flux density at maximum current density, obtained from a 3D finite element simulation: the stator teeth are close to saturation

TABLE II SET GEOMETRY PARAMETERS FOR MANUFACTURE OF THE PROTORYPE

Variable	Description	Values	Unit
d_{sa}	stator outer diameter	266	mm
d_{ri}	rotor inner diameter	134	mm
d_{ri}	rotor bore diameter	118	mm
w_{rs}	back yoke width	13	mm
w_{sz}	stator tooth width	11,75	mm
w_{pm}	magnet width	8,5	mm
w_{sat}	saturation bar width	0,5	mm
w_{rz}	rotor tooth width	19,7	mm
α_{rz}	rotor tooth angle	8	°
l_{pm}	magnet length	54	mm
laminated iron material		M330-35A	
magnetic material		NdFeB N38	

operation (set points of bearing forces and motor torque). The referring simulation results are depicted in Fig. 10. The curves show nearly constant characteristics over the rotor angle. This indicates that the chosen opposing coil connection to create bearing forces and motor torque independently, their linear superposition and the nonlinear decoupling method using the $\mathbf{K}_L(\varphi_r)$-matrix work satisfactory in most cases. Only when all phases are energized to create maximum torque and maximum force at once, indicated by the green dashed lines in Fig. 10, problems arise and the decoupling method deteriorates due to reluctance forces caused by armature reaction, represented in (1) by the part with quadratic dependency from the stator currents. Fortunately, this point of operation is outside the required operational range.

6.2 Characteristic Data

The expected electromagnetic characteristic data of the optimized bearingless flux-switching slice motor is summarized in Table III. At maximum current density a force capacity of about 30N and a drive torque of 1.5Nm can be reached. These values can even be exceeded for short times, e. g. during start-up, when the rotor has to be lifted from its mechanical auxiliary bearings. However, it is

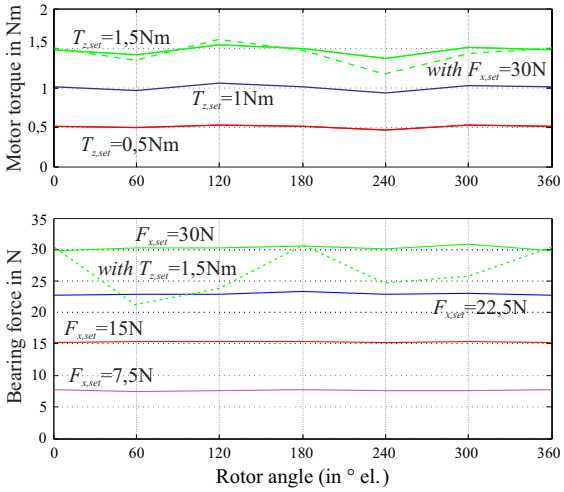

Figure 10. Simulated force and torque creation over the rotor angle: the impressed phase coil currents have been computed from the referring set values of force and torque by the help of the derived $\mathbf{K}_I(\varphi_r)$-matrix

TABLE III ELECTROMAGNETIC CHARACTERISTIC DATA

Variable	Description	Value	Unit
k_r	radial stiffness	-41.6	N/mm
k_z	axial stiffness	7.3	N/mm
k_φ	tilt stiffness	21.4	Nm/rad
J_{max}	max. curr. density	6	A/mm²
F_{max}	max. bear. force	30	N
T_{max}	max. drive torque	1.5	Nm

remarkable that these values lie in the range of comparable standard bearingless slice motors that feature permanent magnets in the rotor [18].

7 Summary and Outlook

In this work the general applicability of the bearingless flux-switching slice motor has been shown theoretically and was confirmed with finite elements simulations. However, it has to be mentioned that only a few slice motor topologies feature an acceptable bearingless motor operation. When single-phase torque operation is acceptable, the amount of possible motor topologies increases significantly.

Furthermore, it was confirmed by finite element simulations, that the air gap between rotor and stator has to remain small in comparison to the stator magnets width to avoid fringing. The demanded small air gap is normally given in standard drives but might be problematic in hermetically sealed bearingless motors that need to have a process chamber wall in the air gap.

Due to the flux concentration capability, the geometric dimensions have to be selected thoughtfully, because of saturation effects that will lead to a loss of linearity of torque and force generation and therefore result in problems with decoupling in the proposed control scheme.

The design of a bearingless flux-switching slice motor prototype is finished. The components have been ordered and are under construction. After the assembly of the system, it is planned to measure

the force and torque characteristic on our test rig and compare the measured data to the simulation results. When the expected behaviour is confirmed, the prototype will be put into full operation.

Acknowledgement

Parts of this work were supported by the Austrian Center of Competence in Mechatronics (ACCM) GmbH, a K2-centre of the COMET program of the Austrian Government. The authors thank the Austrian and Upper Austrian Government for their support.

References

[1] J. Bichsel, *"Beiträge zum lagerlosen Elektromotor"* PhD Nr. 9303, ETH Zürich, 1990

[2] A. Chiba, D. T. Power, M. A. Rahman, *"No load characteristics of a bearingless induction motor"*, Conf. Rec. IEEE IAS Annual Meeting, pp. 126-132, 1991

[3] A. O. Salazar, A. Chiba, T. Fukao, *"A review of developments in bearingless motors"*, Proc. 7th Int. Symp. on Magnetic Bearings (ISMB), pp. 335-340, 2000

[4] R. Schöb, N. Barletta, *"Principle and application of a bearingless slice motor"*, Proc. 5th Int. Symp. on Magnetic Bearings (ISMB), pp. 333-338, 1996

[5] J. Asama, T. Fukao, A. Chiba, M. A. Rahman, T. Oiwa, *"A design consideration of a novel bearingless disk motor for artificial hearts"*, Proc. 1st IEEE Energy Conversion Congress and Exposition (ECCE), pp. 1693-1699, 2009

[6] T. Nussbaumer, K. Raggl, P. Boesch, J. W. Kolar, *"Trends in integration for magnetically levitated pump systems"*, Proc. Power Conversion Conf. (PCC), pp. 1551-1558, 2007

[7] T. Nussbaumer, P. Karutz, F. Zürcher, J. W. Kolar, *"Magnetically levitated slice motors—an overview"*, IEEE Trans. on Industry Applications, vol. 47, no. 2, pp. 754-766, 2011

[8] K. Raggl, J. W. Kolar, T. Nussbaumer, *"Comparison of winding concepts for bearingless pumps"*, Proc. 7th Int. Conf. on Power Electronics (ICPE), pp. 1013-1020, 2007

[9] W. Gruber, W. Briewasser, M. Rothböck, R. Schöb, *"Bearingless slice motor concepts without permanent magnets in the rotor"*, Proc. IEEE Int. Conf. on Industrial Technology (ICIT), pp. 259-265, 2013

[10] W. Gruber, M. Rothböck, R. Schöb, *"Design of a novel homopolar bearingless slice motor with reluctance rotor"*, Proc. 5th IEEE Energy Conversion Congress and Exposition (ECCE), 2013, accepted for publication

[11] S. Rauch, L. Johnson, *"Design principles of flux-switch alternators"*, Power Apparatus and Systems, Trans. of the American Institute of Electrical Engineers, vol. 74, no. 3, part III, pp. 1261–1268, 1955

[12] E. Hoang, A. H. Ben-Ahmed, J. Lucidarme, *"Switching flux permanent magnet poly-phase synchronous machines"*, Proc. 7th European Conf. on Power Electronics and Applications, vol. 3, pp. 903-908, 1997

[13] S. Silber, W. Amrhein, *"Force and Torque Model for Bearingless PM Motors"*, Proc. Int. Power Electronics Conf. (IPEC), vol. 1, pp. 407-411, 2000.

[14] S. Silber, W. Amrhein, *"Power Optimal Current Control Scheme for Bearingless PM Motors"*, Proc. 7th Int. Symp. on Magnetic Bearings (ISMB), pp. 401-406, 2000

[15] J. T. Chen, Z. Q. Zhu, A. S. Thomas, D. Howe, *"Optimal combination of stator and rotor pole numbers in flux-switching pm brushless ac machines"*, Proc. Int. Conf. on Electrical Machines and Systems (ICEMS), pp. 2905-2910, 2008

[16] Z. Q. Zhu, Y. Pang, D. Howe; S. Iwasaki, R. Deodhar, A. Pride, *"Analysis of electromagnetic performance of flux-switching permanent-magnet machines by nonlinear adaptive lumped parameter magnetic circuit model"*, IEEE Trans. on Magnetics, vol. 41, no. 11, pp. 4277-4287, 2005

[17] Z. Q Zhu, Y. Pang, J. Chen, Z. P. Xia, D. Howe, *"Influence of design parameters on output torque of flux-switching permanent magnet machines"*, Proc. 2008 IEEE Vehicle Power and Propulsion Conference (VPPC), pp. 1-6, 2008

[18] W. Gruber, S. Silber, W. Amrhein, T. Nussbaumer, *"Design variants of the bearingless segment motor"*, Proc. Int. Symp. on Power Electronics, Electrical Drives, Automation and Motion (SPEEDAM), pp. 1448-1453, 2010